NRC·CNRC

NRC Publications Archive
Archives des publications du CNRC

Predictive models for the added mass of model ice floes using supervised learning

Seidl, Marius; Murrant, Kevin A.; Quinton, Bruce W. T.; Vardy, Andrew

This publication could be one of several versions: author's original, accepted manuscript or the publisher's version. / La version de cette publication peut être l'une des suivantes : la version prépublication de l'auteur, la version acceptée du manuscrit ou la version de l'éditeur.

For the publisher's version, please access the DOI link below./ Pour consulter la version de l'éditeur, utilisez le lien DOI ci-dessous.

Publisher's version / Version de l'éditeur:

https://doi.org/10.1016/j.coldregions.2026.104951

Cold Regions Science and Technology, 248, C, pp. 1-11, 2026-04-14

NRC Publications Archive Record / Notice des Archives des publications du CNRC :

https://nrc-publications.canada.ca/eng/view/object/?id=77b5acd7-5348-4f23-bc04-984e3d919dd8

https://publications-cnrc.canada.ca/fra/voir/objet/?id=77b5acd7-5348-4f23-bc04-984e3d919dd8

Access and use of this website and the material on it are subject to the Terms and Conditions set forth at

https://nrc-publications.canada.ca/eng/copyright

READ THESE TERMS AND CONDITIONS CAREFULLY BEFORE USING THIS WEBSITE.

L'accès à ce site Web et l'utilisation de son contenu sont assujettis aux conditions présentées dans le site

https://publications-cnrc.canada.ca/fra/droits

LISEZ CES CONDITIONS ATTENTIVEMENT AVANT D'UTILISER CE SITE WEB.

Questions? Contact the NRC Publications Archive team at PublicationsArchive-ArchivesPublications@nrc-cnrc.gc.ca. If you wish to email the authors directly, please see the first page of the publication for their contact information.

Vous avez des questions? Nous pouvons vous aider. Pour communiquer directement avec un auteur, consultez la première page de la revue dans laquelle son article a été publié afin de trouver ses coordonnées. Si vous n'arrivez pas à les repérer, communiquez avec nous à PublicationsArchive-ArchivesPublications@nrc-cnrc.gc.ca.

National Research Council Canada | Conseil national de recherches Canada

Canada

Cold Regions Science and Technology 248 (2026) 104951

Contents lists available at ScienceDirect

Cold Regions Science and Technology

journal homepage: www.elsevier.com/locate/coldregions

Predictive models for the added mass of model ice floes using supervised learning

Marius Seidl [a,*], Kevin A. Murrant [b], Bruce W.T. Quinton [a], Andrew Vardy [a,*]

[a] Memorial University of Newfoundland, St. John's, Canada
[b] National Research Council – Ocean, Coastal and River Engineering, St. John's, Canada

ARTICLE INFO

Keywords:
Model ice
Hydrodynamic coefficients
Added mass
Kinematic simulation
Supervised learning

ABSTRACT

Hydrodynamic effects need to be considered to achieve high fidelity in kinematic simulations of ice floes. Interactions with the surrounding fluid give rise to added mass, which can be modelled by coefficients proportional to the acceleration of the moving ice floe. These coefficients are usually obtained from simple heuristics, model testing or via computational fluid dynamics. However, heuristics are usually restricted to simple geometries and based on significant simplifications, while model testing and computational fluid dynamics are both complex and time-consuming, making all approaches impractical for the accurate and efficient simulation of ice fields with a large number of floes having diverse geometries. Here, we create a dataset of added mass coefficients of prismatic model ice floes floating horizontally at still water level using a boundary element method and introduce two machine learning models for the prediction of the added mass tensors of floes from their geometries. By analyzing general trends in the dataset, we find that changes to the floe geometry systematically affect the tensors and that different tensor entries dominate during undisturbed motions and during collisions. The introduced machine learning models are capable of predicting any individual entry of the learned tensors with less than 1% error, with the convolutional neural network being able to predict added mass for floes of all tested geometries. Our approach enables the kinematic simulation of large and complex model ice fields.

1. Introduction

Computer simulation is a versatile tool for the analysis of ships navigating icy waters. It can be used for the development and testing of autopilots in these harsh environments (Pearson et al., 2023), for the calculation of ice loads on ship hulls (Daley et al., 2012; Daley et al., 2014; Alawneh et al., 2015; Polojärvi and Tuhkuri, 2009; Gong et al., 2019; Polojärvi et al., 2021; Lubbad et al., 2018; Hahn et al., 2017; Huisman et al., 2019) as well as other structures (Morgan et al., 2015; Morgan, 2016), and for the analysis of the temporal evolution of ice fields under the influence of ships traversing them (De Schaetzen et al., 2023). Simulations for these purposes have been recently reviewed by Islam et al. (2021) as well as Li and Huang (2022).

Generally, kinematic simulations are used to predict the motions of objects over time. For objects floating on water, hydrostatic and hydrodynamic effects need to be modelled for a high-fidelity simulation. It is common practise to augment the governing equations of motion with factors modelling the added mass caused by the fluid (Fossen, 2002). For ships and other floating structures, these factors can be determined from heuristics, via computer simulation or in model tests. Current heuristics are either derived from experimental data or first principles and, for the most part, rely on significant generalizations and simplifications to cover a wide range of cases (Zhang et al., 2019). While efficient, they are inherently less accurate than more intricate approaches and thus not well-suited for high-fidelity kinematic simulations. Computer simulations to determine hydrodynamic coefficients exist in various flavours. However, any computational fluid dynamics (CFD) code relies on specifically prepared and sophisticated three-dimensional models of the geometry of the floating object in question (Zikanov, 2019; Tu et al., 2023). This and the high computational costs make CFD difficult to apply and computationally expensive. Additionally, the obtained results are only valid for the one analyzed model. Model testing requires elaborate experimental equipment and the manufacturing of a physical scale model of the floating object to be characterized (ITTC, 2021). Thus, neither of the latter methods is feasible for naturally occurring floating objects like sea ice, since the variety of properties and geometries of these natural objects, which may even change over time, makes the preparation of computational or physical models impractical.

* Corresponding authors.
E-mail addresses: mseidl@mun.ca (M. Seidl), av@mun.ca (A. Vardy).

https://doi.org/10.1016/j.coldregions.2026.104951
Received 30 June 2025; Received in revised form 23 December 2025; Accepted 12 April 2026
Available online 14 April 2026
0165-232X/© 2026 The Author(s). Published by Elsevier B.V. This is an open access article under the CC BY-NC-ND license (http://creativecommons.org/licenses/by-nc-nd/4.0/).

This paper introduces an approach to derive added mass coefficients for model ice floes floating horizontally at still water level solely based on their shape and thickness in an efficient manner via machine learning (ML). The boundary element method (BEM) of the WAMIT (WAMIT, Inc, 2025) software package was used to create a dataset of the added mass coefficients of polygonal prisms resembling the shape variety of model ice floes. With data solely generated by a BEM, deviations between the dataset and the properties of real model ice floes must be expected. Though, a basic validation against experimental data indicates the general usefulness of the computationally produced data. Thus, general trends of the influence of floe shape and thickness on the added mass coefficients were identified and discussed. As the main focus of this work, supervised ML models that are capable of predicting the added mass tensors from the two-dimensional shape and thickness of a floe with high accuracy were trained on the created dataset. These ML models are essentially sophisticated heuristics for the estimation of added mass tensors of model ice floes that eliminate the need to prepare intricate three-dimensional models of the floe. The prediction quality achievable by the ML models is primarily limited by the physical accuracy of the dataset. Two different families of ML models were derived. A shallow feed-forward neural network model family (NN models) is lightweight and takes the vertex coordinate of the floe's polygonal shape as input. However, this family of models is only applicable to polygons with a fixed number of vertices, such that a different model is needed for each number of vertices. Thus, a large number of models from this family is required to cover the complete dataset, and a new model is required for any new type of floe shape. The alternative convolutional neural network model family (CNN models) takes a binary image of the polygonal shape of a model ice floe as input. This enables the models of this family to generalize over different polygonal shapes. Using the CNN models, only a single model is needed to predict each feature of the created dataset. Since images of a polygon can be created from vertex coordinates (as is done in this work) and vertex coordinates can be extracted from images of polygons, the input formats are basically interchangeable. Thus, the core difference between the two model families is that the NN models are computationally less expensive but less general, while the CNN models are computationally more expensive but more general. Due to this trade-off, both model families were explored in this work. Ultimately, it is shown that both types of models can predict added mass tensors of model ice floes from the dataset with high accuracy. Ultimately, the ML models enable the efficient kinematic simulation of large and complex model ice fields based on appropriate added mass tensors.

Early approaches to estimate the added mass for a given floating object relied on data obtained for simple geometries and applied these factors to the object of interest. Within strip theory, the 3D geometry is broken down into two-dimensional planar sections and analytical solutions for the added mass for these sections are found based on fundamental theory. The values for the three-dimensional body are then constructed from the solutions of the plane sections (Lewis, 1989; Newman, 2017). In the so-called method of equivalent ellipsoids, the object to be analyzed is matched with an ellipsoid, for which theoretical solutions are known (Korotkin, 2009).

Due to proximity effects and large accelerations, it is expected that the added mass is different during a collision event compared to undisturbed maneuvering (Korotkin, 2009). In the limit of instantaneous collisions, the added mass at infinite frequency should be used (Motora et al., 1969). Based on theoretical calculations and model testing, early work proposed constant added mass (CAM) factors for the different degrees of freedom during collisions of ships, which have been used to model ship-ice collisions (Minorsky, 1959; Motora, 1960; Motora et al., 1969; Petersen, 1982; Petersen and Pedersen, 1981; Zhang et al., 2019).

Over time, different models have been developed to estimate the added mass of ice floes. They can be classified as being theoretical (i.e. based on first-order theory), experimental, or computational, with recent trends going towards the use of the latter. However, even in recent work, CAM approaches are still being used, due to their simplicity and efficiency (Kim et al., 2017; Song et al., 2016; Yang et al., 2021).

An early theoretical model was described by Popov et al., who introduced a set of equations to calculate the properties of polygonal ice floes from their geometries (Popov et al., 1967). Luk (1987) used long water wave theory to derive added mass over a wide variety of conditions, including collisions, for circular ice floes. Isaacson and Cheung (1988) used potential theory to investigate the effect of proximity between two cylindrical ice pieces on the added mass of the individual pieces. In 1999, (Daley, 1999) extended the work by Popov et al. (1967) to create the so-called Popov-Daley method, which became highly influential for modelling ship-ice collisions. Zong and Zhou (2019) introduced a model based on shape factors to estimate the hydrodynamic properties of polygonal ice floes. Jiang et al. (2022) describe an approach to interactively calculate the added mass of circular ice floes during ship-ice interactions using potential theory.

Recent experimental results include the work of Frederking and Timco (2000), who used model-scale sea ice to investigate the kinematics of floe-floe interactions in a test tank study. McGovern and Bai (2014) characterized the kinematics of square model ice floes in regular waves. Experimental results were also obtained for circular ice floes by Meylan et al. (2015). They used ice floes made out of polymer at a $1:100$ scale, equipped with a motion tracking system, and focused particularly on the surge motion of the floes in waves. Their results have also been successfully used by Yiew et al. (2016) in a theoretical model. A similar experimental approach with polygonal polymer model ice of different shapes at a $1:50$ scale was used by Zhao et al. (2023) to determine the added mass coefficients in surge during collisions with a circular object.

Computational fluid dynamics approaches to modelling the added mass and kinematics of ice floes have been very common in recent years (Song et al., 2016; Li and Huang, 2022). Most commonly, the added mass of individual ice floes is not explicitly calculated and used in a separate kinematic simulation but integrated in the CFD calculations (Chen et al., 2024; Huang et al., 2020; Lee and Nguyen, 2010; Wang and Derradji-Aouat, 2010). However, Tsarau et al. (2014) used a BEM and designed a quadrilateral mesh for each ice floe of interest to calculate its added mass explicitly.

The remainder of this manuscript is structured as follows: Section 2 introduces the methodology used in this work. Results are shown and discussed in Section 3. The paper closes with a summary and conclusion (Section 4).

2. Methods

A dataset of $100,000$ polygonal prisms representing model ice floes was created by drawing $10,000$ convex n-gon shapes with $n \in [3, 4, \ldots, 11, 12]$ each from a random polygon distribution using Wolfram Mathematica (Wolfram Mathematica, 2025). Each polygon was assigned a random orientation from a uniform distribution and a random diameter from an exponential distribution with a mean of 1m, cutoff at 0.1m as the lowest value. The polygons were then extruded to prisms with random thicknesses drawn from a uniform distribution over the interval $[0.01\text{m}, 0.20\text{m})$ but limited to half the polygon's diameter. The resulting prisms are oriented with the polygonal faces in the x-y plane and the extrusion along the z-axis, thus representing floes floating horizontally at the still water level. From a density of $930\,\text{kg/m}^3$ (assumed to be uniform throughout the whole floe) for EGADS model ice (Spencer and Timco, 1990) and $1002.5\,\text{kg/m}^3$ for liquid EGADS (Hill and Kirby, 1995), the submerged portion of the floes was calculated to be 92.8%. EGADS is an aqueous solution named after its ingredients Ethylene Glycol, Aliphatic Detergent and Sugar, which mimics the properties of sea ice on a model scale when frozen (Spencer and Timco, 1990; Hill and Kirby, 1995). Fig. 1 demonstrates the described geometric situation.

Based on the symmetry of the floes, their centre of gravity (CG) was

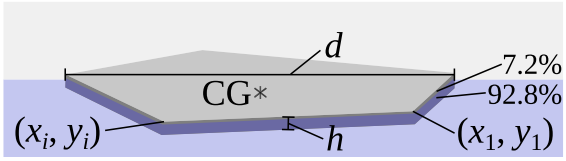

Fig. 1. Geometry and properties of a polygonal prism representing a model ice floe and its orientation with respect to the free surface.

determined. The x- and y-components coincide with the centroid of the polygon, and the z-component is located at 50% of the thickness of a floe. With the known CG, the distance from CG to the waterline was calculated for each individual floe. The inertia tensor for each floe was determined by voxelizing the floe at a resolution of $1/100$ of its diameter and integrating over the mass distribution of all voxels, assuming a uniform density. From the inertia tensor, the signed radius of gyration tensor was calculated. A quadrilateral mesh of each polygonal prism representing a model ice floe was created using gmsh's (gmsh, 2025) *simple* meshing and *simple* recombination algorithm leading to an automatically determined mesh resolution with typically 100–1000 faces per mesh. Note that the output of the used boundary element method (WAMIT Inc, 2025) is virtually independent of the mesh resolution in the present special case of polygonal prisms, since they consist of perfectly flat faces and straight edges only.

The quadrilateral mesh, the previously calculated signed radius of gyration tensor, and the geometrically obtained distance from CG to the waterline were used as the only required inputs to the WAMIT computational package (WAMIT Inc, 2025) to calculate the zero and infinite wave frequency added mass tensor. These wave frequencies were selected due to their usefulness for kinematic simulations. The added mass at zero wave frequency is a good approximation for undisturbed maneuvering (i.e. ice floes moving freely in the absence of proximity effects), while the added mass at infinite wave frequency can be used to resolve instantaneous collisions (Motora et al., 1969). In conclusion, the created dataset maps the polygonal shape and thickness of each polygonal prism representing a model ice floe to its added mass tensors under the given conditions.

The PyTorch library (PyTorch, 2025) was used to implement two families of ML models. Firstly, a family of shallow feed-forward neural networks (NN) with ReLu activation function was used. Models from this family are tailored to one value of n only. The size of the hidden layer and the learning rate of the NN models were determined separately for each output using a grid search based on the 7-gon dataset (Section 3). For each type of n-gon, three separate models were optimized with $2n + 1$ inputs ($2n$ vertex coordinates and thickness) and either one of the two added mass tensors (each 36 elements) as output. Secondly, a convolutional neural network (CNN) was combined with a shallow feed-forward NN (Fig. 2). A single CNN model is suitable for multiple values of n at the same time. The convolution part of the CNN models consists of two convolution layers with two maximum pooling layers and ReLU activation function. The details of the layers are shown in Table 1.

The convolution part of the CNN model turns a 128×128 pixel image input (see below) into an $8 \times 8 \times 32 = 2048$ flattened feature vector. The CNN design is loosely inspired by LeNet (Bottou et al., 1994) and AlexNet (Krizhevsky et al., 2017). The 2048 extracted features together with the pixel size of the input image and the thickness of the floe serve as the 2050 inputs to the shallow feed-forward NN part of the model, which uses the same hidden layer size determined in the grid search for the NN model family for a given output. A separate model of the CNN model family was trained for each added mass tensor. For all models, the mean squared error (MSE) loss criterion was selected, and the parameters were optimized using an Adam optimizer. The batch size was set to 100, and the number of epochs to $20,000$ and $30,000$ for the feed-forward NN models for added mass at zero wave frequency and added mass at infinite wave frequency, respectively and to 250 for the CNN-based models, to guarantee a stabilized loss upon termination. All inputs and outputs of the model were normalized as follows. For the polygon vertices, a single normalization parameter was used to achieve all vertex coordinates $\in [-1, 1]$. Thickness and all output dimensions were normalized individually to a $[0, 1]$ range. The performance of each ML model was evaluated by a 10-fold cross-validation.

To create the input images for the CNN model from the vertex coordinates of the n-gons, a 128×128 pixel grid was set up with a size to just fit the polygon, including a 5% padding along its longer axis, and the polygon was fitted to the image as a binary black-white value by a point (i.e. pixel) in polygon test for each pixel. Thus, for each polygon, a 128×128 black-and-white image was created with a unique (and square) pixel size.

3. Results and discussion

3.1. Dataset validation and properties

The dataset (https://github.com/mseidl92/model-ice-ML/tree/main/dataset) created for this work is a first of its kind, as it makes

Table 1
Details of the layers used for the convolution part of the CNN models.

layer	kernel size	stride	padding	output size
1st convolution layer	11	4	5	$32 \times 32 \times 16$
1st max pooling layer	2	2	–	$16 \times 16 \times 16$
2nd convolution layer	5	1	2	$16 \times 16 \times 32$
2nd max pooling layer	2	2	–	$8 \times 8 \times 32$

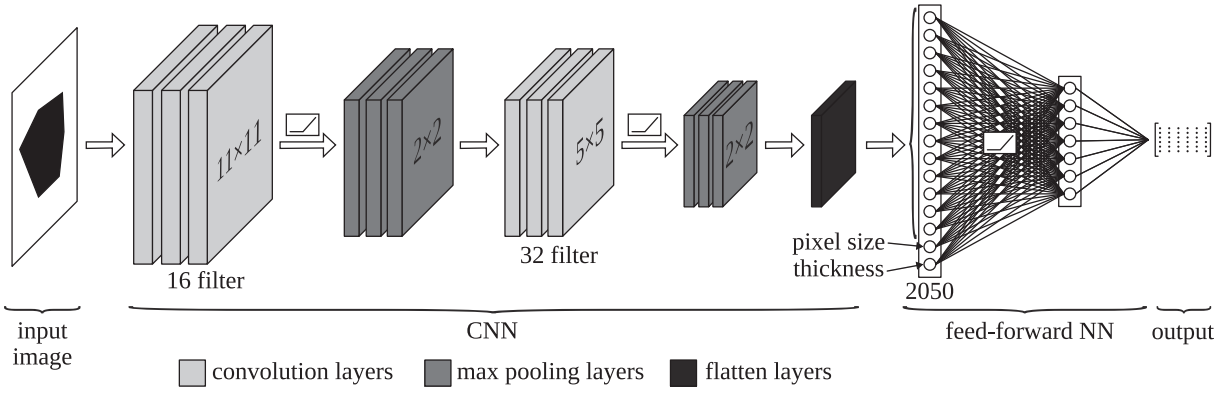

Fig. 2. Design of the model combining a CNN with a shallow feed-forward NN to predict added mass tensors from an 128×128 image of the ice floe's polygonal shape, the image's pixel size, and the floe's thickness.

estimates of full added mass tensors for a wide variety of polygonal prisms resembling the shape variety of model ice floes available. It should be noted that the obtained coefficients are solely the output of a BEM (WAMIT Inc, 2025) and, as such, deviations between the dataset and the properties of real model ice floes must be expected. Unfortunately, experimental data of full added mass tensors of model ice floes to validate our dataset against is lacking in the literature. As a basic validation, the added mass coefficients C_m experimentally obtained by Zhao et al. (2023) for the surge motion of model ice floes of different shapes and sizes during collision events were compared to the outputs of WAMIT at zero and infinite wave frequency for the same floes under the same motion (Fig. 3). The outputs of WAMIT are in good agreement with the experimentally observed trends of decreasing added mass coefficients with increasing floe size d and number of vertices n. Moreover, the experimentally observed range of added mass coefficients (depending on data evaluation method) falls within the range of WAMIT's outputs for zero and infinite wave frequency. This is to be expected since added mass should be increased during collision events compared to undisturbed motions (i.e. zero wave frequency) (Korotkin, 2009). That the added mass coefficients computed by WAMIT for infinite wave frequency are not reached during the experiments can be explained by the duration of the collisions. In fact, Zhao et al. (2023) reported a prolonged collision period for their experiments, explaining the small difference to the added mass coefficients produced by WAMIT for zero wave frequency. The maximum added mass produced at infinite wave frequency would be reached during an instantaneous collision only.

The good agreement between experimental and computed data indicates the usefulness of our dataset. However, the validation is limited to only 1 of the 36 entries of the full added mass tensor making up the dataset. Despite this limitation, the dataset is a result in itself and was analyzed statistically to identify systematic trends in the computed added mass coefficients. For this purpose, the individual entries of the added mass tensors were treated separately. Figs. 4 and 5 show the probability density distributions of the nondimensionalized diagonal elements of the added mass tensors for zero and infinite wave frequency, respectively. Nondimensionalization of the added mass values to their respective added mass coefficients C_m is achieved through division by the floe's mass for surge, sway, and heave or the corresponding entry of the moment of inertia tensor for roll, pitch, and yaw. The distributions are given as a function of the number of vertices of the polygons n, as well as the ratio h/d between floe thickness h and floe diameter d representing the relative thickness of a floe. The latter was categorized in intervals of 0.1, leading to 5 categories based on the constraints used for the floe geometry (Section 2). An overview of the different observed trends is given in the following text, while the full account for each of the 36 entries of the added mass tensors is shown in Figs. A1 and A2 in the appendix. Since a coherent nondimensionalization is impossible for the non-diagonal elements of the added mass tensors, the data given in the appendix is not nondimensionalized. The data is also individually scaled due to the different units and physical meanings of the different entries. To increase visual comparability by limiting the data range, outliers were removed from all shown distributions (Figs. 4, 5, A1, and A2) based on Tukey's criterion (Tukey, 1977) with a constant of 0.5 for the interquartile range.

Looking at the added mass tensors at zero wave frequency (Fig. 4), distributions of the strictly positive values with varying degrees of asymmetry are found for all nondimensionalized diagonal elements. Due to the random orientation of the floes in the dataset, the distributions for surge and sway, as well as roll and pitch, are virtually identical and henceforth discussed together as surge/sway and roll/pitch. For surge/sway and yaw, the spread, asymmetry, and mean of these distributions decrease continuously with the number of vertices. This decrease of spread and asymmetry is much faster for heave, where the distributions are almost symmetrical and stable for $n \geq 5$, while undergoing a slight increase in mean. For roll/pitch, a similar trend of quick stabilization of spread and asymmetry with $n \geq 5$ is observed, while the means neither increase nor decrease but only stabilize.

These observed trends are attributed to the change in the general shape of the floes with the increase in the number of vertices. Convex polygons with a low number of vertices are more likely to be wedge-shaped, while a higher number of vertices produces more round and ellipsoidal shapes. This explains the decrease of the added mass coefficients for surge/sway and yaw, since more round polygonal shapes generally lead to lower interactions of the rectangular sides of the floe with the fluid upon surge/sway motions and yaw rotations. The increase in surface area at constant diameter of a convex polygon with increasing number of vertices can explain why the mean added mass coefficient increases slightly for heave and stabilizes for roll/pitch with the increasing number of vertices. The volume of fluid that must be moved upon these motions increases, but so does the mass of the floe. With more similar shapes at larger n, both effects balance more, leading to more stable distributions. The general decrease in shape variety with increasing number of vertices can further explain the general decrease in asymmetry observed in almost all distributions in Fig. 4.

Considering the influence of the relative floe thickness, the mean added mass coefficients as well as their spread increase for surge/sway and yaw with h/d, while both trends are generally reversed for heave and roll/pitch. Only for the roll/pitch added mass coefficients of triangles, the spread of the distributions increases with relative floe thickness.

With increased relative thickness of a floe, the rectangular side faces of the prism representing the floe have more relative surface area compared to the top and bottom faces. As described for the general trends, these side faces convey the main interaction with the fluid during surge/sway and yaw motions, thus explaining the observed increase of added mass coefficients with h/d. On the contrary, the main interaction for heave and roll/pitch motions is between the bottom polygonal face and the fluid. This face does not change with relative thickness and thus only a small effect on the added mass coefficient is expected. The increase of the floe's mass with increased thickness at constant polygonal shape, together with the nondimensionalization of the added mass

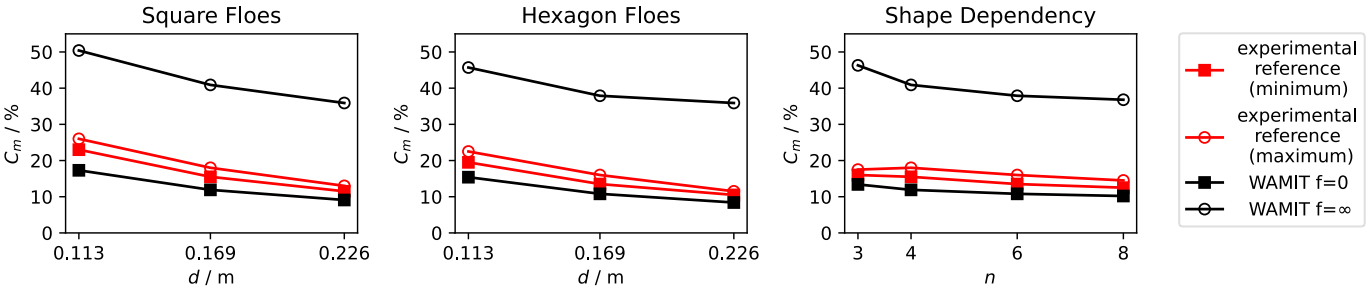

Fig. 3. Comparison between the added mass coefficients experimentally obtained by Zhao et al. (2023) and the outputs from WAMIT used to compose the dataset used in this study. Good agreements between experimental and computed data are observed for the trends obtained for square (left) and hexagonal floes (center) of different sizes, as well as floes of different shapes (right).

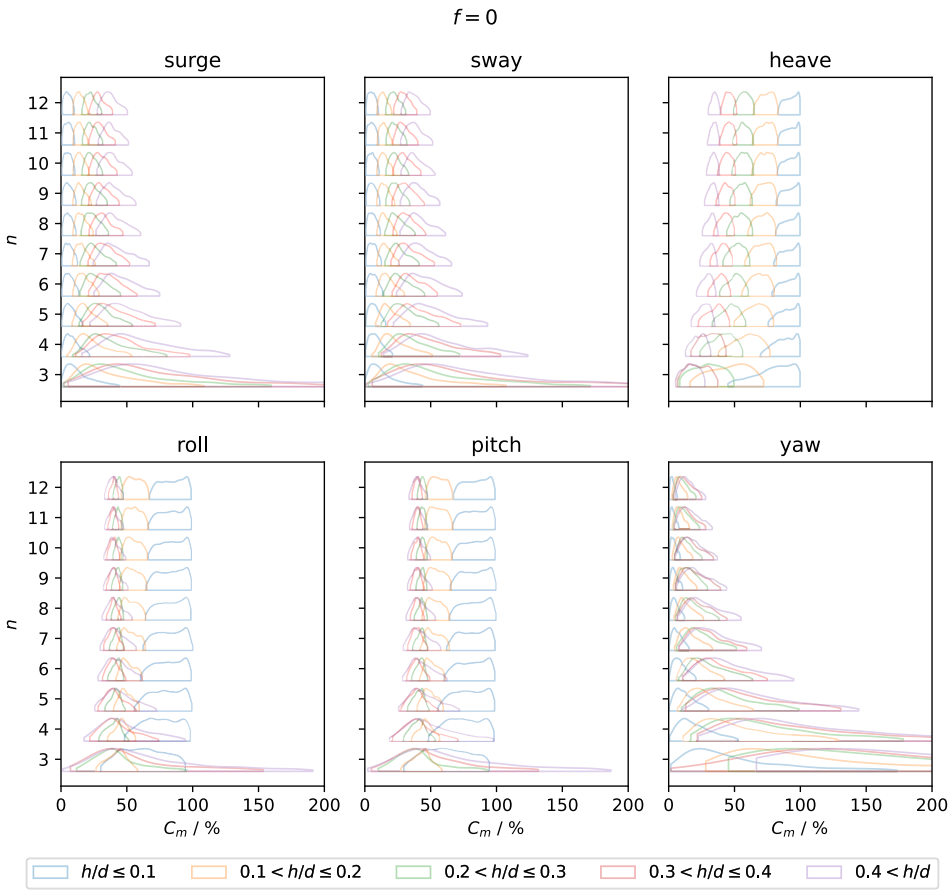

Fig. 4. Probability density distributions of the nondimensionalized diagonal entries of the added mass tensor at zero wave frequency as a function of the number of vertices n, categorized by the ratio of floe thickness and diameter h/d, as indicated by the legend. Details of the data preparation are given in the main text.

coefficients, thus explains the observed trend. The significantly stronger asymmetry of the distributions of floes with higher relative thickness at small n can probably be attributed to the requirement that floes are at most half as thick as their diameter. More asymmetric polygons would simply be extruded to these larger relative thicknesses more often.

The absolute values of the off-diagonal elements of the added mass tensors at zero wave frequency (Fig. A1) are between one and four orders of magnitude smaller than those of the diagonal elements. For all off-diagonal values except the surge-pitch and sway-roll couplings, a symmetric distribution with zero mean is observed. For most elements (surge-sway, surge-roll, surge-yaw, sway-pitch, sway-yaw, heave-roll, heave-pitch, heave-yaw, roll-yaw, and pitch-yaw couplings), the width of the distributions decreases with the number of vertices. For the surge-heave, sway-heave, and roll-pitch couplings, the width instead increases.

From these trends together with the magnitudes of the different off-diagonal values (Fig. A1), it can be concluded that the surge-sway, surge-pitch, sway-roll, and roll-pitch couplings are the most significant off-diagonal factors influencing the motions of model ice floes. As such, these entries of the added mass tensor should not be ignored when trying to create high-fidelity motion models.

For the added mass tensors at infinite wave frequency (i.e. during instantaneous collision events (Motora et al., 1969)), the same fundamental trends of the distribution shapes and changes with the number of vertices are observed (Figs. 5 and A2). However, the observed distributions are generally more spread out and asymmetric and thus generally less stable, indicating more extreme values in the distributions compared to the zero wave frequency results. Additionally, the mean values of all tensor entries are increased to different degrees as follows. For the surge/sway and yaw entries as well as the surge-sway, surge-roll, surge-yaw, sway-pitch, sway-yaw, and heave-yaw couplings, the increase is low and in the range of twofold to fourfold and generally similar for the different h/d categories. The entries for heave, as well as the surge-heave, surge-pitch, sway-heave, sway-roll, roll-yaw, and pitch-yaw couplings are increased 10-fold to 20-fold. Increases of more than two orders of magnitude are observed for the roll and pitch entries, as well as the roll-pitch coupling, while even more than three orders of magnitude increases occur for the heave-roll and heave-pitch couplings. Almost all increases in orders of magnitude are more pronounced for relatively thinner floes. It should be noted however, that the rigid body assumption made throughout this work will fail first for these thinnest floes and effects like floe splitting, rafting, and ridging become more prevalent.

The vastly different changes in magnitude of the entries of the added mass tensors for zero and infinite wave frequency indicate that it is crucial to use different added mass tensors when simulating free-floating and colliding model ice pieces to create high-fidelity results. The thinner the ice floe relative to its diameter, the more important dedicated added mass values for collision scenarios become. In conclusion, the diagonal values are the most important values of the added mass tensor in either situation. However, the importance of the heave, roll, and pitch entries is significantly enhanced during collision events. Moreover, the roll-pitch, heave-roll, and heave-pitch couplings take over the role of the most influential off-diagonal elements during collisions.

3.2. Feed-forward neural networks

In a first step to predicting the values of the added mass tensors at zero and infinite wave frequency, a grid search was executed to determine the optimal learning rate and hidden layer size for the feed-

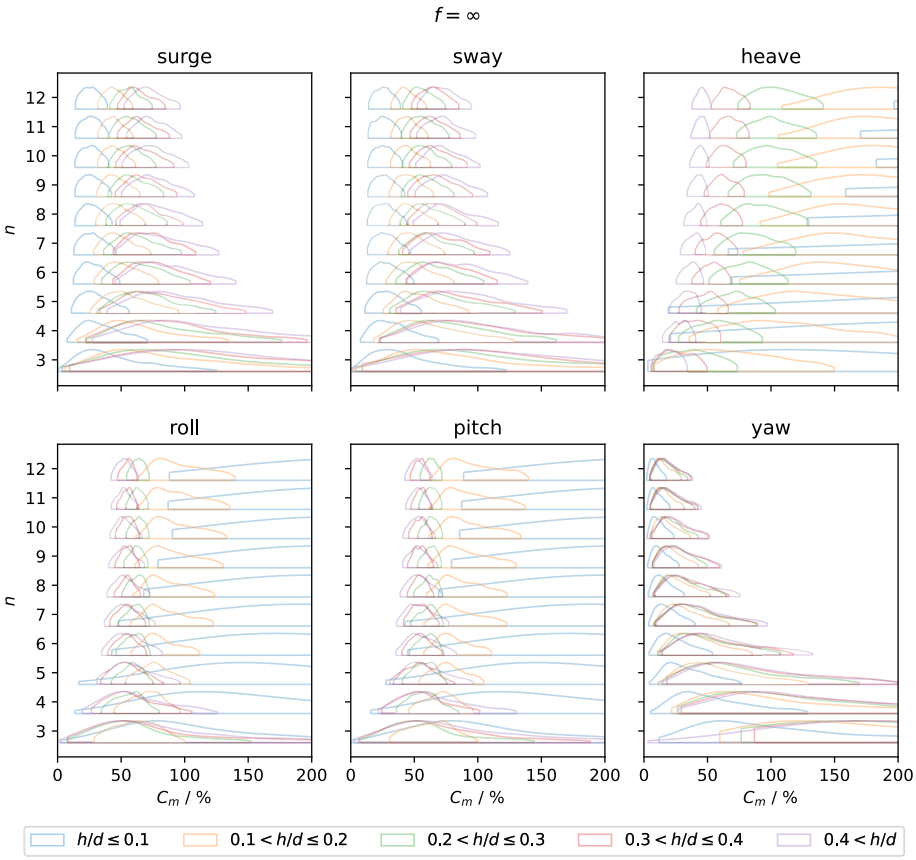

Fig. 5. Probability density distributions of the nondimensionalized diagonal entries of the added mass tensor at infinite wave frequency as a function of the number of vertices n, categorized by the ratio of floe thickness and diameter h/d, as indicated by the legend. Details of the data preparation are given in the main text.

forward neural networks used. Fig. 6 shows the minimal MSE loss obtained over all epochs of training as a function of hidden layer size and learning rate.

For the added mass tensors at zero wave frequency, the learning rate of 10^{-5} produces the smallest losses for each given layer size and thus was chosen for the final models. For the added mass tensors at infinite wave frequency, the learning rate of 10^{-5} was chosen as well, although the smallest loss overall is obtained for a learning rate of 10^{-4} at a layer size of 8192. However, for that learning rate, the trend with respect to increasing layer size is not a systematic decrease as expected. Thus, the more conservative learning rate of 10^{-5} was chosen.

Fig. 7 shows the MSE loss as a function of epoch number for the chosen learning rates, which was used to determine the optimal hidden layer size. For both tensor types, a decrease in the loss with an increase in layer size is observed. For the added mass tensors at zero wave frequency, there are diminishing returns when increasing the layer size above 1024. As such, a layer size of 1024 was chosen to create a more efficient model. The same trend is observed for the added mass tensors at infinite wave frequency, where a layer size of 8192 was chosen, as diminishing returns were reached at that point. It is not surprising that a larger model is required for the added mass tensors at infinite wave frequency, since the analysis of the dataset revealed a larger variation of the individual entries of these tensors. Table 2 summarizes the learning rates and layer sizes used for the different tensor types.

With the determined hyperparameters (Table 2), a separate machine learning model was trained for each added mass tensor type and each number of vertices. The performance of the trained models was assessed by cross-validation. The results of the 10-fold cross-validation are shown in Table 3 as mean cross-validation errors together with their standard deviation.

For a given tensor, the cross-validation errors do not vary significantly beyond their error bounds. From this observation, it can be

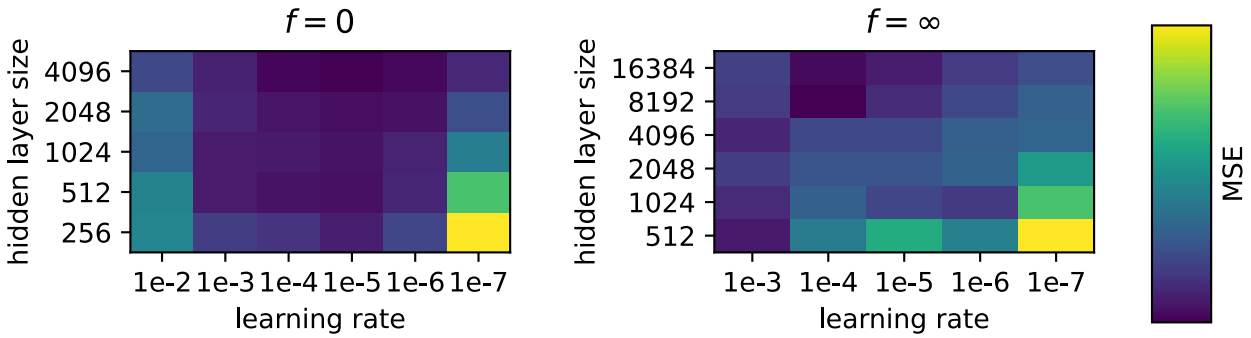

Fig. 6. Minimal MSE loss as a function of learning rate and hidden layer size to predict the added mass tensors from the geometry of ice floes with 7 vertices.

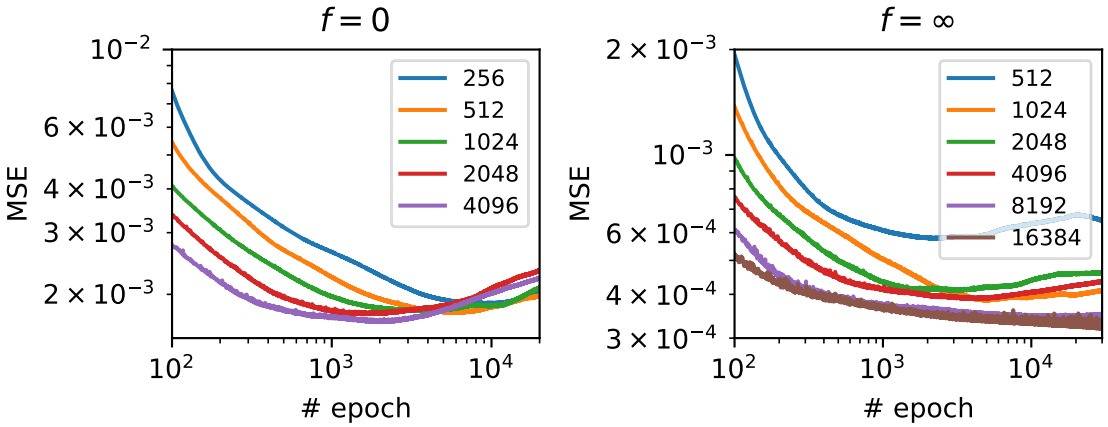

Fig. 7. MSE loss as a function of number of epochs at fixed learning rates as indicated in the main text, with varying hidden layer sizes for the different added mass tensor types in the dataset for polygons with 7 vertices.

Table 2
Used parameters for the supervised learning of the two different types of added mass tensors as determined by grid search.

	$f = 0$	$f = \infty$
learning rate	10^{-5}	10^{-5}
hidden layer size	1024	8192

Table 3
Mean cross-validation errors with standard deviation for the different added mass tensor types and numbers of vertices n.

n	$f = 0$	$f = \infty$
3	0.0020 ± 0.0005	0.0002 ± 0.0002
4	0.002 ± 0.001	0.0003 ± 0.0003
5	0.002 ± 0.001	0.0005 ± 0.0005
6	0.0031 ± 0.0006	0.0006 ± 0.0004
7	0.0026 ± 0.0005	0.0005 ± 0.0001
8	0.0030 ± 0.0008	0.0007 ± 0.0003
9	0.0027 ± 0.0005	0.0009 ± 0.0009
10	0.0022 ± 0.0003	0.0005 ± 0.0001
11	0.0028 ± 0.0005	0.001 ± 0.003
12	0.0027 ± 0.0009	0.001 ± 0.002

concluded that the determined hyperparameters (i.e. layer size and learning rate) are valid for all numbers of vertices analyzed. Additionally, the observed standard deviations of the errors indicate that the models are not overfitting the data and that using the smallest hidden layer size when obtaining diminishing returns was appropriate. That most cross-validation errors for either tensor type are below 0.003 indicates that the models perform well in predicting the tensors, since the entries were normalized to $[0, 1]$ range for the machine learning. Thus, the cross-validation errors indicate less than 0.3% average deviation between the true and predicted value for all entries of a given added mass tensor.

3.3. Convolutional neural networks

The most significant drawback of the family of models based on feed-forward NNs is the need for a separate model for each number of vertices. In an actual ice field, it can be expected that there are floes of different shapes that must be modelled by polygons with different numbers of vertices. As such, a better approach would produce a single model that can predict the tensors for floes of different shapes. For that purpose, the CNN-based models were introduced, which take an image of an ice floe as input, extract features from this image, and feed those features into a feed-forward NN to finally predict the tensor of interest. As such, the model can handle inputs from different polygonal shapes and potentially beyond that.

Fig. 8 shows the MSE loss for the CNN-based models for all folds of the cross-validation. From the cross-validation, the mean errors and standard deviations were obtained as 0.0066 ± 0.0004 for the added mass tensors at zero wave frequency and 0.0032 ± 0.0006 for the added mass tensors at infinite wave frequency.

With 0.3–0.7% average error for the prediction of a single entry of any given tensor, the CNN-based models perform similarly to the models based on a feed-forward NN. However, the CNN-based models inherently generalize better than the feed-forward NNs, since they can predict the added mass tensors of ice floes with a larger diversity (i.e. any number of vertices n). Since a list of vertices can simply be turned into an input image for the CNN-based model, it is expected that the CNN-based model will be preferable for most applications, unless computationally small and fast models are needed, in which case the feed-forward NNs are preferable. Moreover, the image input will be preferable for situations in which the added mass of real model ice floes should be estimated. Experimentally obtained images can be turned into valid inputs for the CNN-based model without the need to extract vertex information by pure image segmentation techniques. As such, the range of potential applications of the CNN-based models exceeds that of the feed-forward NNs.

4. Summary and conclusion

This work introduced a new dataset of added mass coefficients for a wide variety of polygonal prisms resembling the shape variety of model ice floes. The dataset was produced using a boundary element method. A basic validation for the surge added mass coefficients revealed good agreement between experimental and computed data. Systematic changes of the added mass coefficients with the number of vertices of the ice floe, as well as the relative floe thickness, were analyzed. It was confirmed that the diagonal elements of the added mass tensors are the dominant elements. However, depending on the situation (i.e. undisturbed motions versus collisions), different coupling terms in the added mass tensors become highly influential as well. Changes in added mass for these different situations are more pronounced for thinner floes.

On the dataset, two different families of machine learning models were trained to predict the added mass tensors from the geometry (i.e. shape and thickness) of a model ice floe. For a shallow feed-forward neural network, hyperparameters were determined using a grid search, and with the tuned hyperparameters, a model was trained for each tensor type and number of vertices of the polygon. With these models' errors below 0.3% for the prediction of a single entry of each tensor were obtained.

Finally, the CNN-based models were trained to predict the added

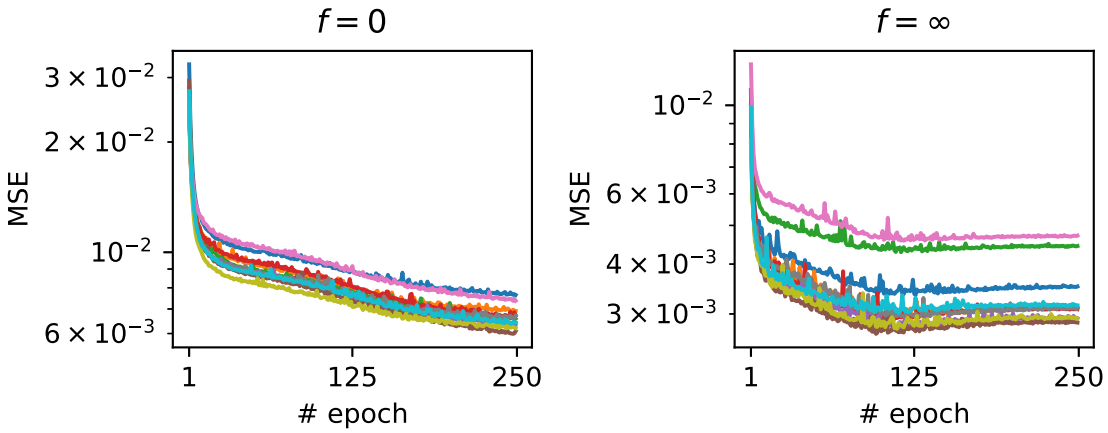

Fig. 8. MSE loss as a function of the number of epochs during 10-fold cross-validation for the CNN-based models.

mass tensor of interest without needing a separate model for each number of vertices. The CNN part of the model extracts features from an image of the polygon. These features, together with the image pixel size and the floe's thickness, are used in a shallow feed-forward NN to predict the entries of the added mass tensors. With this more general approach, errors between 0.3 and 0.7% for the prediction of a single entry of the given tensors were achieved.

In future work, the introduced dataset should be validated against experimental data of real model ice floes for additional degrees of freedom. Since it was shown that the introduced ML models can predict the values of the dataset with high accuracy, the quality of the models' outputs hinges on the quality of the underlying dataset. Thus, obtaining the needed experimental data for this validation is a crucial next step. Once sufficiently validated, the analysis of the dataset could be extended, ideally to derive conclusions on the single floe level instead of the distribution level. Adding data for intermediate wave frequencies to the dataset would be desirable as well, since such data would enable the development and training of more capable ML models for the prediction of added mass tensors at any desired wave frequency. Moreover, a similar dataset could be generated for tensors describing other hydrodynamic effects like damping. However, this would require more involved CFD calculations to be executed on a large number of objects as well as additional experimental validation to draw real-world conclusions. Finally, the generalization ability of the CNN-based models could be tested beyond the introduced dataset. For example, circular, ellipsoid or non-convex polygons could be used as input to the existing model to see if the model generalizes even to these shapes it has never seen before.

CRediT authorship contribution statement

Marius Seidl: Writing – review & editing, Writing – original draft, Visualization, Software, Methodology, Investigation, Formal analysis, Data curation, Conceptualization. **Kevin A. Murrant:** Supervision, Funding acquisition. **Bruce W.T. Quinton:** Writing – review & editing, Resources, Project administration, Methodology. **Andrew Vardy:** Writing – review & editing, Supervision, Funding acquisition.

Declaration of competing interest

The authors declare that they have no known competing financial interests or personal relationships that could have appeared to influence the work reported in this paper.

Acknowledgements

The authors thank Heather Peng for the fruitful discussions. We are further grateful to the Ocean Frontier Institute for their financial support of Marius Seidl in the framework of the Ocean Graduate Excellence Network.

Appendix A. Full distributions of added mass tensor entries

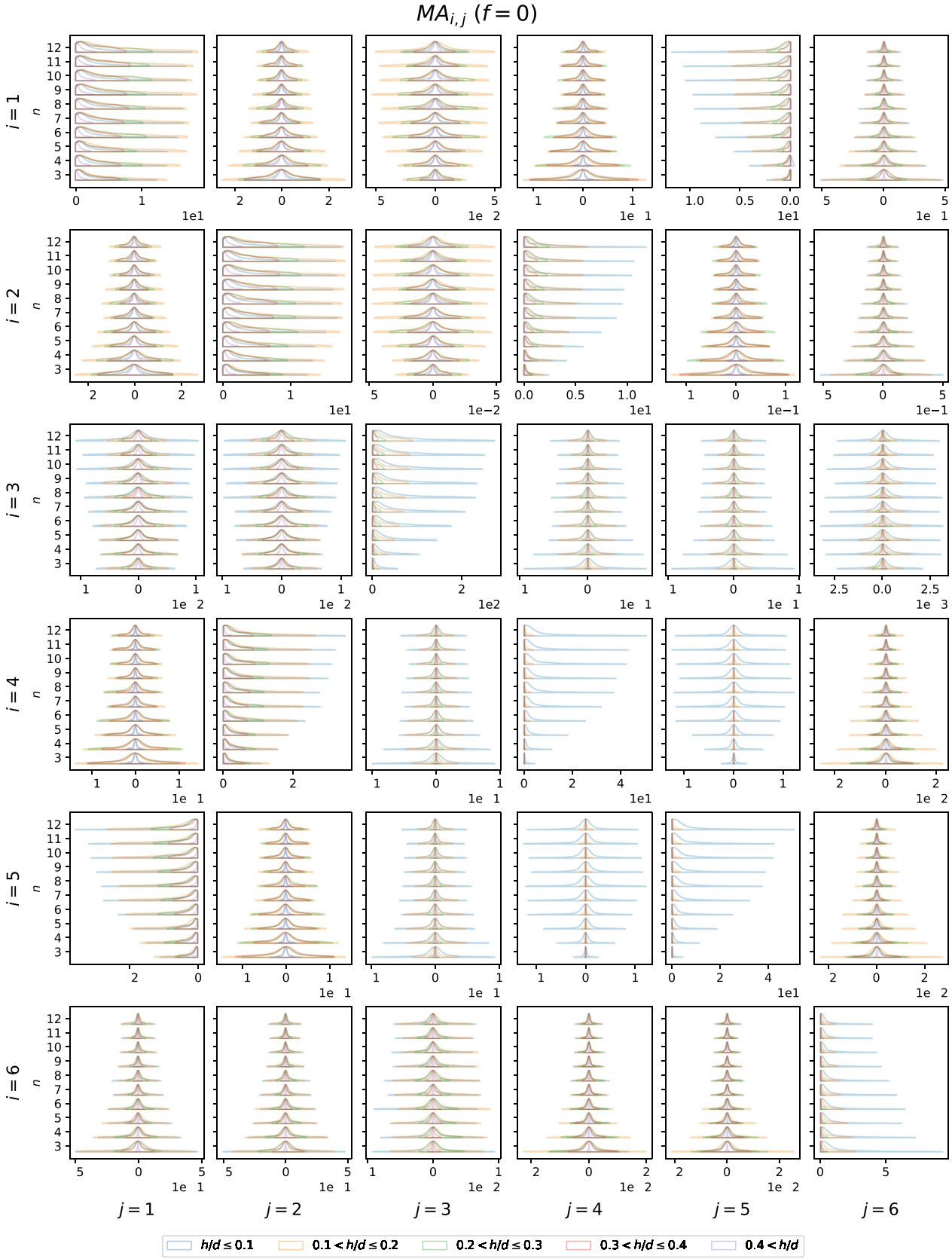

Fig. A1. Probability density distributions of all 36 entries of the added mass tensor at zero wave frequency in standard tensor order as a function of the number of vertices n, categorized by the ratio of floe thickness and diameter h/d, as indicated by the legend. The added mass values are not nondimensionalized and scaled independently per matrix entry. Details of the data preparation are given in the main text.

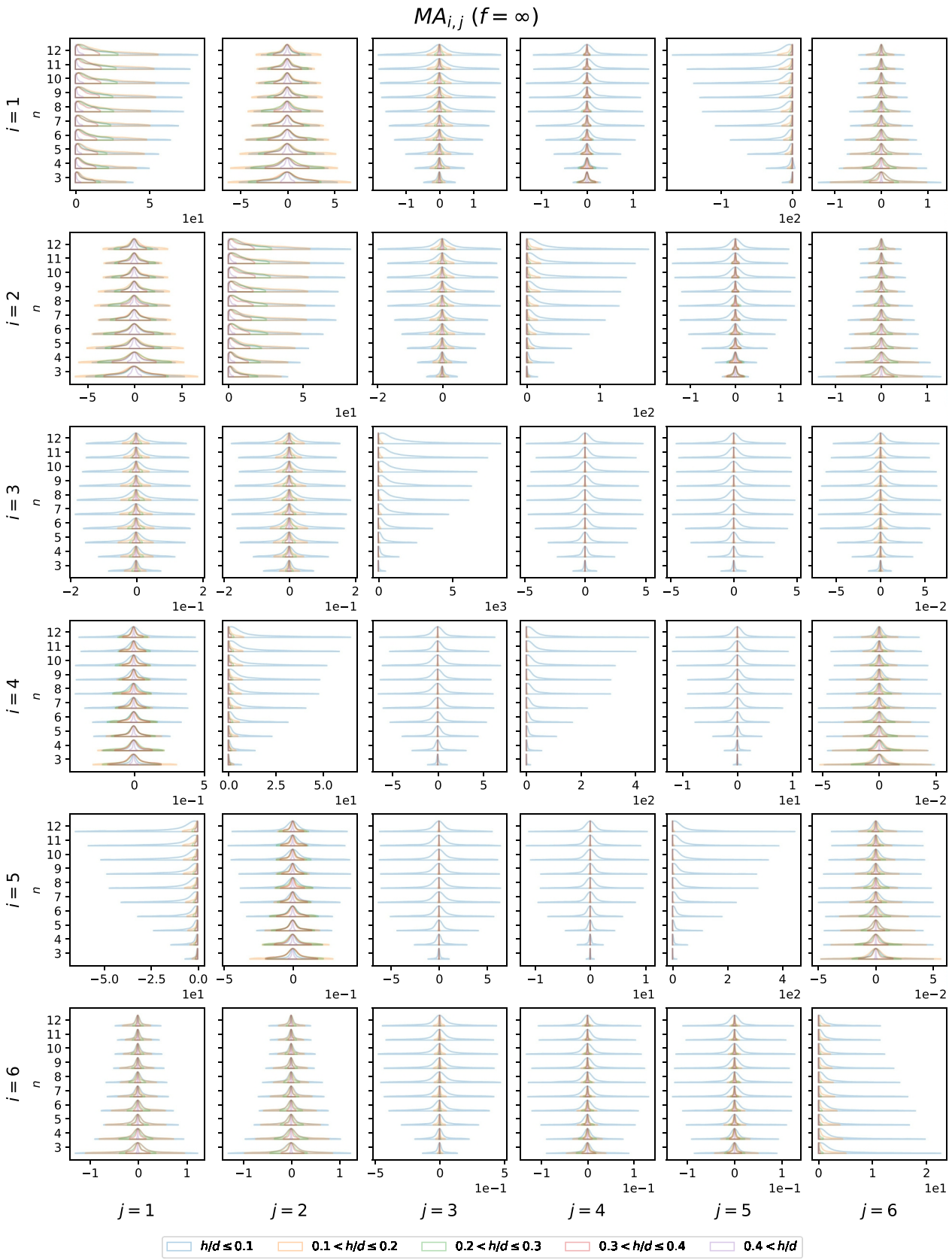

Fig. A2. Probability density distributions of all 36 entries of the added mass tensor at infinite wave frequency in standard tensor order as a function of the number of vertices n, categorized by the ratio of floe thickness and diameter h/d, as indicated by the legend. The added mass values are not nondimensionalized and scaled independently per matrix entry. Details of the data preparation are given in the main text.

Data availability

The created dataset and the best performing machine learning models are available at https://github.com/mseidl92/model-ice-ML.

References

Alawneh, S., Dragt, R., Peters, D.K., Daley, C., Bruneau, S., 2015. Hyper-Real-Time ice simulation and modeling using GPGPU. IEEE Trans. Comput. 64 (12), 3475–3487.

Bottou, L., Cortes, C., Denker, J.S., Drucker, H., Guyon, I., Jackel, L.D., LeCun, Y., Muller, U.A., Sackinger, E., Simard, P., Vapnik, V., 1994. Comparison of classifier methods: A case study in handwritten digit recognition. In: Proceedings of the 12th IAPR International Conference on Pattern Recognition. 2, pp. 77–82.

Chen, J., Chen, Z., Wang, D., Zhang, Y., He, Y., 2024. Prediction and empirical formula correction for brash ice resistance using CFD-DEM based on invisible bulbous bow ship. Ocean Eng. 310 (2), 118752.

Daley, C., 1999. Energy based ice collision forces. In: International Conference on Port and Ocean Engineering under Arctic Conditions.

Daley, C., Alawneh, S., Peters, D., Quinton, B., Colbourne, B., 2012. GPU modeling of ship operations in pack ice. In: Proceedings of the 10th International Conference and Exhibition on Performance of Ships and Structures in Ice, pp. 1–6.

Daley, C., Alawneh, S., Peters, D., Colbourne, B., 2014. GPU-event-mechanics evaluation of ice impact load statistics. OTC Arct. Technol. Conf. 1–11.

De Schaetzen, R., Botros, A., Gash, R., Murrant, K., Smith, S.L., 2023. Real-time navigation for autonomous surface vehicles in ice-covered waters. In: IEEE International Conference on Robotics and Automation, pp. 1069–1075.

Fossen, T.I., 2002. Marine Control Systems – Guidance, Navigation, and Control of Ships, Rigs and Underwater Vehicles. Marine Cybernetics.

Frederking, R., Timco, G., 2000. Sea ice floe impacts - large scale basin experiments. In: Proceedings of the Tenth International Offshore and Polar Engineering Conference, pp. 640–645.

GMSH, 2025. A Three-Dimensional Finite Element Mesh Generator With Built-In Pre- And Post-Processing Facilities (Online, accessed February 18, 2025).

Gong, H., Polojärvi, A., Tuhkuri, J., 2019. Discrete element simulation of the resistance of a ship in unconsolidated ridges. Cold Reg. Sci. Technol. 167, 102855.

Hahn, M., Dankowski, H., Ehlers, S., Erceg, S., Rung, T., Huisman, M., Sjöblom, H., Leira, B.J., Chai, W., 2017. Numerical Prediction of Ship-Ice Interaction: A Project Presentation. International Conference on Ocean, Offshore and Arctic Engineering.

Hill, B., Kirby, C.S., 1995. Open Water Resistance Tests in the Ice Tank: A Comparison of EGADS and Fresh Water. National Research Council of Canada. Institute for Marine Dynamics. Technical Paper.

Huang, L., Tuhkuri, J., Igrec, B., Li, M., Stagonas, D., Toffoli, A., Cardiff, P., Thomas, G., 2020. Ship resistance when operating in floating ice floes: a combined CFD&DEM approach. Mar. Struct. 74, 102817.

Huisman, M., Erceg, S., von Bock Polach, R.U.F., Rung, T., Ehlers, S., 2019. Numerical Simulation of Ship-Ice Interaction. International Conference on Ocean, Offshore and Arctic Engineering.

International Towing Tank Conference, 2021. ITTC - Recommended Procedures and Guidelines, 10th Revision. Technical Paper.

Isaacson, M., Cheung, K.F., 1988. Influence of added mass on ice impacts. Can. J. Civ. Eng. 15, 698–708.

Islam, M., Mills, J., Gash, R., Pearson, W., 2021. A literature survey of broken ice-structure interaction modelling methods for ships and offshore platforms. Ocean Eng. 221, 108527.

Jiang, Z., Li, F., Mikkola, T., Kujala, P., Hirdaris, S., 2022. The influence of added mass in ship-ice-wave interactions: a potential flow hydromechanics model. In: Proceedings of the ASME 2022 41st International Conference on Ocean, (Offshore and Arctic Engineering).

Kim, E., Storheim, M., Amdahl, J., Loset, S., von Bock und Polach, R.U.F., 2017. Laboratory experiments on shared-energy collisions between freshwater ice blocks and a floating steel structure. Ships Offshore Struct. 12 (4), 530–544.

Korotkin, A.I., 2009. Added Masses of Ship Structures. Springer-Verlag.

Krizhevsky, A., Sutskever, I., Hinton, G.E., 2017. ImageNet classification with deep convolutional neural networks. Commun. ACM 60 (6), 84–90.

Lee, S. G., Nguyen, H.A., 2010. LNGC collision response analysis with iceberg considering surrounding seawater. In: Proceedings of the 20th International Offshore and Polar Engineering Conference, 206e14.

Lewis, E.V., 1989. Principles of Naval Architecture Volume III - Motions in Waves and Controllability. Society of Naval Architects and Marine Engineers.

Li, F., Huang, L., 2022. A review of computational simulation methods for a ship advancing in broken ice. J. Mar. Sci. Eng. 10, 165.

Lubbad, R., Løset, S., Lu, W., Tsarau, A., van den Berg, M., 2018. Simulator for Arctic Marine Structures (SAMS). International Conference on Ocean, Offshore and Arctic Engineering.

Luk, C.-H., 1987. Added mass and damping for ice floes by long water wave theory. J. Waterw. Port Coast. Ocean Eng. 113 (5), 447–463.

McGovern, D.J., Bai, W., 2014. Experimental study on kinematics of sea ice floes in regular waves. Cold Reg. Sci. Technol. 103, 15–30.

Meylan, M.H., Yiew, L.Y., Bennetts, L.G., French, B.J., Thomas, G.A., 2015. Surge motion of an ice floe in waves: comparison of a theoretical and an experimental model. Ann. Glaciol. 56 (69), 155–159.

Minorsky, V., 1959. An analysis of ship collisions with reference to protection of nuclear power plants. J. Ship Res. 1–4.

Morgan, D., 2016. An Improved Three-Dimensional Discrete Element Model for Ice Structure Interaction (International Symposium on Ice).

Morgan, D., Sarracino, R., McKenna, R., Thijssen, J.W., 2015. Simulations of ice rubbling against conical structures using 3D DEM. In: International Conference on Port and Ocean Engineering Under Arctic Conditions.

Motora, S., 1960. On the Measurement of Added Mass and Added Moment of Inertia of Ships in Steering Motion. Technical Paper.

Motora, S., Fujino, M., Sugiura, M., Sugita, M., 1969. Equivalent added mass of ship in collision. J.S.N.A. Japan 126 (10), 138–148.

Newman, J.N., 2017. Marine Hydrodynamics. MIT Press.

Pearson, W., Islam, M., Lau, M., Gash, R., Mills, J., 2023. Discrete event simulation of vessel stationkeeping operations in ice-rich waters. SIMULATION 99 (7), 729–753.

Petersen, M.J., 1982. Dynamics of ship collisions. Ocean Eng. 9 (4), 295–329.

Petersen, M.J., Pedersen, P., 1981. Collisions Between Ships and Offshore Platforms. (Offshore Technology Conference).

Polojärvi, A., Tuhkuri, J., 2009. 3D discrete numerical modelling of ridge keel punch through tests. Cold Reg. Sci. Technol. 56 (1), 18–29.

Polojärvi, A., Tuhkuri, J., Gong, H., 2021. Comparison of full-scale and DEM simulation data on ice loads due to floe fields on a ship hull. In: International Conference on Port and Ocean Engineering under Arctic Conditions.

Popov, Y., Faddeyev, O., Kheisin, D., Yalovlev, A., 1967. Strength of Ships Sailing in Ice. Sudostroenie Publishing House.

PyTorch, 2025. PyTorch Documentation. https://pytorch.org/docs/stable/index.html online, accessed February 18, 2025.

Song, M., Kim, E., Amdahl, J., Ma, J., Huang, Y., 2016. A comparative analysis of the fluid-structure interaction method and the constant added mass method for ice-structure collisions. Mar. Struct. 49, 58–75.

Spencer, D.S., Timco, G.W., 1990. CD Model Ice - a Process to Produce Correct Density (CD) Model Ice, IAHR Ice Symposium..

Tsarau, A., Lubbad, R., Loset, S., 2014. A numerical model for simulation of the hydrodynamic interactions between a marine floater and fragmented sea ice. Cold Reg. Sci. Technol. 103, 1–14.

Tu, J., Yeoh, G.H., Liu, C., Tao, Y., 2023. Computational Fluid Dynamics: A Practical Approach. Elsevier.

Tukey, J.W., 1977. Exploratory Data Analysis. Addison-Wesley.

WAMIT, Inc 2025. WAMIT USER MANUAL version 7.5. Https: //www.wamit.com/manual7.x/v75_manual.pdf (online, accessed february 18, 2025).

Wang, J., Derradji-Aouat, A., 2010. Ship Performance in Broken Ice Floes: Preliminary Numerical Simulations. Technical Paper. National Research Council of Canada. NRC Institute for Ocean Technology.

Wolfram Mathematica, 2025. RandomPolygon. Https: //reference.wolfram.com/language/ref/RandomPolygon.Html.En (online, accessed february 18, 2025).

Yang, B., Sun, Z., Zhang, G., Wang, Q., Zong, Z., Li, Z., 2021. Numerical estimation of ship resistance in broken ice and investigation on the effect of floe geometry. Mar. Struct. 75, 102867.

Yiew, L.Y., Bennetts, L.G., Meylan, M.H., French, B.J., Thomas, G.A., 2016. Hydrodynamic responses of a thin floating disk to regular waves. Ocean Model 97, 52–64.

Zhang, S., Pedersen, P.T., Villavicencio, R., 2019. Probability and Mechanics of Ship Collision and Grounding. Butterworth-Heinemann.

Zhao, Y., Sun, Z., Zhang, G., Yang, B., Yang, B., 2023. Experimental and numerical studies on hydrodynamic effects of ice floe drift and impact process in uniform current. Cold Reg. Sci. Technol. 216, 104011.

Zikanov, O., 2019. Essential Computational Fluid Dynamics. John Wiley & Sons.

Zong, Z., Zhou, L., 2019. A theoretical investigation of ship ice resistance in waters covered with ice floes. Ocean Eng. 186, 106114.